Radiation Due to a Convex Curvature Discontinuity of a Dielectric-Coated Perfect Conductor

David H. Monteith and Robert G. Olsen

***Abstract*—Surface waves radiate energy at discontinuities in the curvature of the guiding structure. By reciprocity, surface waves will be excited by plane waves incident upon such a discontinuity. Here, the problem of the radiation of a surface wave on a flat dielectric-coated perfect conductor incident upon an abrupt change to a dielectric-coated cylindrical conductor with a large radius of curvature is considered. The problem is formulated as an integral equation over the aperture of the discontinuity. Since the change in curvature is modest, an approximate perturbation solution to the integral equation is derived and the radiated field due to the discontinuity is found. This radiated field reduces to published results for an impedance surface approximation when that approximation is valid. The problem of mode conversion and associated radiation near higher mode cutoffs is also studied. It is found that near mode cutoffs, the higher order mode dominates the radiation pattern and causes the overall radiation pattern due to the discontinuity in curvature to be narrow and end fire. Away from cutoff, when all of the propagating bound modes are more tightly bound to the surface, the radiation pattern is less narrow and less end fire. For very tightly bound modes the pattern is nearly uniform. For dielectrics characterized by small permitivities, the changes in radiation pattern should be measurable.**

***Index Terms*—Electromagnetic radiation, electromagnetic scattering.**

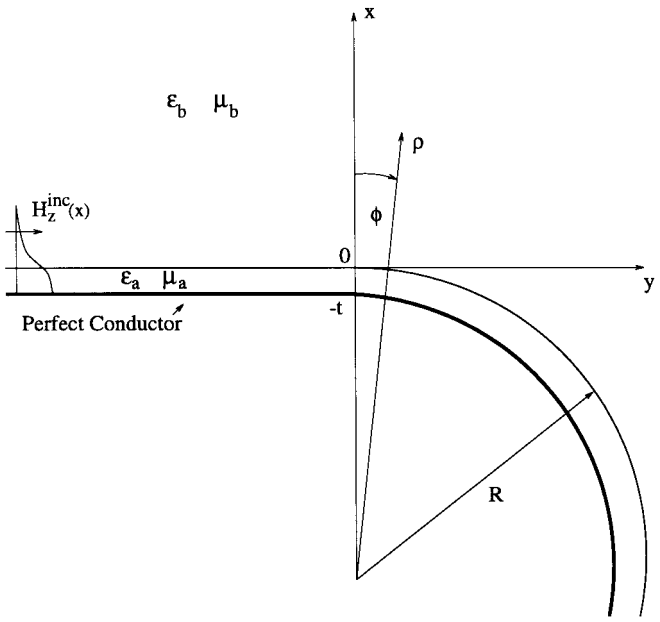

Fig. 1. The problem geometry.

I. Introduction

BOUND modes of open waveguides radiate energy at irregularities such as an abrupt change in curvature [1]. By reciprocity, a plane wave incident upon such an irregularity will excite a bound mode. An important problem is to determine the extent of this coupling and if it is affected by operating close to a higher mode cutoff frequency of the waveguide.

A few authors have considered what occurs at an abrupt change in curvature. Most notably, Weston [2], [3] and Senior [4] solved for the fields near the junction of two electrically large parabolic perfectly conducting cylinders and from this they also solved for the scattered field due to the junction discontinuity. Shevchenko [1] and Kuester and Chang [5], extended the problem to an impedance surface, solving for the radiation due to a straight impedance surface abruptly changing to a convex curved impedance surface characterized by a large radius of curvature.

To determine how operation close to a higher order mode cutoff frequency affects coupling, a more complex structure must be considered. The structure considered in this paper is a dielectric-coated perfect electric conductor with an abrupt but modest change in curvature. The solution to the problem is formulated as an integral equation over the discontinuity aperture. An approximate solution of this integral equation when the change in radius is modest is developed. This solution is used to compare the radiated field of the coated surface to that predicted using the impedance surface approximation and to look at the radiated field of the coated surface when the operating frequency is near higher mode cutoffs.

Manuscript received June 25, 1996; revised May 26, 1998.

The authors are with the School of Electrical Engineering and Computer Science, Washington State University, Pullman, WA 99164 USA.

Publisher Item Identifier S 0018-926X(98)06105-5.

II. Problem Statement

The problem is to solve for the radiation due to a TM surface wave incident upon an abrupt convex curvature discontinuity of a dielectric-coated perfect conductor. The two-dimensional (2-D) problem is considered.

The problem geometry is shown in Fig. 1. In general, both sides of the discontinuity could be curved, but for simplicity, one side was chosen to be flat. The dielectric is assumed to be homogeneous, isotropic, and linear and is characterized by permitivity $\varepsilon_0\varepsilon_a$ and permeability $\mu_0\mu_a$ and thickness t. The region above the dielectric is also homogeneous, isotropic, and linear and is characterized by the constitutive parameters $\varepsilon_0\varepsilon_b$ and $\mu_0\mu_b$. The radius of curvature of the curved section is R. To avoid the necessity of dealing with a second discontinuity

in curvature, it is assumed that the flat section ranges from $y = 0$ to $y \to -\infty$. It is also assumed that the curved section ranges from $\phi = 0$ to $\phi \to \infty$ in a kind of Riemann surface of which only finite angles of ϕ lie in the physical plane [6]. This artifice is similar in intent to the assumption of infinite extent of a straight waveguide in an excitation problem and assures that none of the scattered fields are reflected from some obstacle further along the structure [5].

The incident field H_z^{inc} is a TM surface wave supported by an infinite planar dielectric-coated perfect conductor. By reciprocity, the solution also applies to the excitation of surface waves by plane waves incident upon the curvature discontinuity. Of special interest is the large radius case. A time dependence of $\exp(j\omega t)$ is assumed where $\omega = 2\pi f$ is the angular frequency and f is the frequency in Hertz.

III. Problem Formulation

Examination of the problem geometry, Fig. 1, shows that the abrupt curvature discontinuity can be used to define an semi-infinite aperture on the plane $y = 0$ and $x > -t$. An integral equation for the unknown fields across the aperture can be formulated in a manner similar to Rayleigh and Sommerfeld's formulation of an integral equation to solve for diffraction due to a finite aperture [7].

A. Integral Equation Formulation

The derivation of the integral equation begins by applying the 2-D Green's identity (1) to the regions on either side of the aperture. This identity is a statement of reciprocity for the scalar fields ψ and ϕ [8]

$$\oint_\ell \left(\psi \frac{\partial \phi}{\partial n} - \phi \frac{\partial \psi}{\partial n}\right) d\ell = \int_A [\psi \nabla^2 \phi - \phi \nabla^2 \psi]\, da \qquad (1)$$

where

$$\begin{aligned} \text{in region } S\text{: } \ell &= \ell_S = \ell_{SR} + \ell_{SP} + \ell_{SC} \\ A &= A_S \\ \vec{n} &= \vec{n}_S \\ \text{in region } C\text{: } \ell &= \ell_C = \ell_{CR} + \ell_{CP} + \ell_{SC} \\ A &= A_C \\ \vec{n} &= \vec{n}_C. \end{aligned}$$

The contours $(\ell_{S,C})$, surface areas $(A_{S,C})$, and outward normals $(\vec{n}_{S,C})$ of the regions being considered are shown in Fig. 2.

To identify the functions ψ and ϕ, the Green's functions in the straight and curved regions G_S and G_C, respectively, are postulated. These Green's functions satisfy the inhomogeneous wave equation, the boundary condition on the perfect electric conductor, the radiation condition and the boundary conditions at the surface of the dielectric coating in the regions S and C, respectively. For each region S and C, there are four Green's functions [9]. One for each permutation of the field point $\vec{\rho}$ and the source point $\vec{\rho}'$ inside the dielectric coating and above the dielectric coating.

Rayleigh and Sommerfeld showed that the problem could be simplified without limiting its generality by introducing

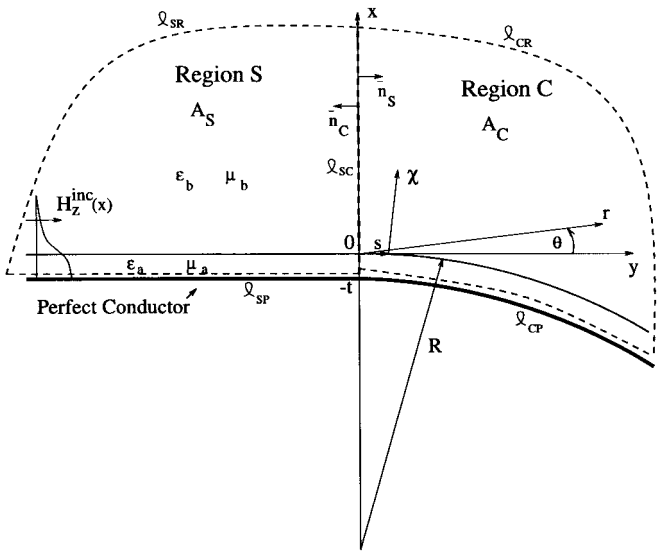

Fig. 2. The regions S and C.

modified Green's functions G_S^* and G_C^* as defined in below [7], [10]:

$$G_{S,C}^*(\vec{\rho}, \vec{\rho}') = G_{S,C}(\vec{\rho}, \vec{\rho}') + G_{S,C}(\vec{\rho}, \vec{\rho}'_{im}) \qquad (2)$$

where

$$\vec{\rho}' = x'\vec{a}_x + y'\vec{a}_y \quad \text{implies} \quad \vec{\rho}'_{im} = x'\vec{a}_x - y'\vec{a}_y.$$

The simplification comes about because the derivative of the modified Green's functions with respect to y' evaluated on the aperture is zero.

Now consider the total magnetic field in the two regions.

- In region S

$$H_z = H_{zS} = H_{zS}^{\text{inc}} + H_{zS}^{\text{scat}} \qquad (3)$$

- In region C

$$H_z = H_{zC}. \qquad (4)$$

These magnetic fields satisfy the homogeneous Helmholtz equation and the boundary conditions. It should be remembered that H_{zS}^{inc} is not arbitrary. It also satisfies the boundary condition and the Helmholtz equation in region S. Hence, H_{zS}, H_{zS}^{inc}, and H_{zS}^{scat} satisfy the boundary conditions and H_{zS}^{scat} also satisfies the radiation condition.

At this point, the quantities ψ and ϕ in the Green's identity (1) for each side of the aperture are defined as follows:

- In region S define

$$\begin{aligned} \psi &= G_S^* \\ \phi &= H_{zS} - H_{zS}^{\text{inc}} = H_{zS}^{\text{scat}}. \end{aligned} \qquad (5)$$

- In region C define

$$\begin{aligned} \psi &= G_C^* \\ \phi &= H_{zC}. \end{aligned} \qquad (6)$$

Applying the boundary condition, the radiation condition, and using the Helmholtz equation and the inhomogeneous wave equation, the Green's identity becomes as follows.

- In region S

$$\int_{\ell_{SC}} \left(G_S^* \frac{\partial H_{zS}^{\text{scat}}}{\partial y'} \right) dx' = \begin{cases} H_{zS}(\vec{\rho}) - H_{zS}^{\text{inc}}(\vec{\rho}) & y \le 0 \\ H_{zS}(\vec{\rho}_{im}) - H_{zS}^{\text{inc}}(\vec{\rho}_{im}) & y \ge 0 \end{cases} \tag{7}$$

- In region C

$$-\int_{\ell_{SC}} \left(G_C^* \frac{\partial H_{zC}}{\partial y'} \right) dx' = \begin{cases} H_{zC}(\vec{\rho}) & y \ge 0 \\ H_{zC}(\vec{\rho}_{im}) & y \le 0. \end{cases} \tag{8}$$

These equations can be further simplified by noting that on the aperture $G_{S,C}^* = 2G_{S,C}$.

For ease of notation, the quantity $f(x')$ is defined as

$$f(x') = \left. \frac{\partial H_z}{\partial y'} \right|_{y'=0}. \tag{9}$$

Thus, $f(x')$ is proportional to the unknown tangential electric field at the aperture. In the current problem, the incident field H_{zS}^{inc} is known, the tangential electric field on the perfect conductor is zero, and the scattered fields satisfy the radiation condition. Thus, by the uniqueness theorem [6], once $f(x')$ is determined, the fields everywhere are uniquely determined.

To determine $f(x')$, continuity of tangential E and H across the aperture are enforced. This results in the following Fredholm integral equation of the first kind for the unknown $f(x')$.

$$\Phi(x) + 2\int_{-t}^{\infty} K_S(x,x') f(x')\, dx' + \int_{-t}^{\infty} [K_C(x,x') - K_S(x,x')] f(x')\, dx' = 0 \tag{10}$$

where

$$K_{S,C}(x,x') = G_{S,C}(x,0;x',0)$$

and $\Phi(x)$ is the known quantity defined as

$$2\Phi(x) = \left\{ -2\int_{\ell_{SC}} G_S \frac{\partial H_{zS}^{\text{inc}}}{\partial y'}\, dx' + H_{zS}^{\text{inc}} \right\}_{y=y'=0}. \tag{11}$$

Since in the given problem the change in curvature is small, the integral equation (10) is written in a perturbation form. The coated surface on one side of the aperture is straight and on the other it is curved with a large radius of curvature R. As the radius of curvature of a cylinder becomes infinite the Green's function for the cylinder will approach the Green's function for the planar surface [11]. Because G_C approaches G_S, it is convenient to write G_C as G_S plus some correction that approaches zero as R approaches infinity. Two possible ways to calculate this perturbation are through the use of a large argument expansion of G_C [10] or through the use of regular perturbation theory [13]. The second approach is much easier to implement. The use of the perturbation form will allow easier calculation of the small changes in the fields that are expected to be associated with the small change in curvature in the present problem.

Equation (10) can be solved to determine the unknown $f(x')$ on the aperture and from this the fields everywhere can be determined by using (7) and (8).

B. Perturbation Formulation

Regular perturbation theory is used to derive a perturbation series representation of the cylindrical Green's function. In this procedure, the cylindrical coordinate system is defined in terms of a local coordinate system χ and s. χ and s are shown in Fig. 2 and are defined in (12) and (13) in terms of the cylindrical coordinates ρ and ϕ, which are shown in Fig. 1.

$$\frac{\rho}{R} = 1 + \xi\chi \tag{12}$$

$$\phi R = s \tag{13}$$

where

$$\xi = \frac{1}{R}.$$

In a small region near the aperture, the local coordinate system χ and s approaches the rectangular coordinate system x and y. This region can be determined by comparing χ, s and x, y leading to the conditions in the following:

$$\left| \frac{\chi}{R} \right| \ll 1 \tag{14}$$

$$\phi \ll 1. \tag{15}$$

The integration in the integral equation (10) extends to infinity and this causes an apparent contradiction with (14). Fortunately, at large distances from the surface, K_C approaches K_S [11] and the difference between the two vanishes. Under these conditions, the second integral of the integral equation can be truncated. Thus, as long as the perturbation equation is accurate out to a distance where the difference between K_C and K_S is negligible, then (14) will not be violated. The difference between K_C and K_S is also negligible at points far from the surface $k\rho \to \infty$. This, along with (12) and (14), leads to the final restriction on the perturbation series

$$\left| \frac{1}{k_{a,b} R} \right| \ll 1. \tag{16}$$

To derive the perturbation form of the Green's functions, they are first expanded as a perturbation series in terms of the variable ξ

$$K_C = K_0 + \xi K_1 + \xi^2 K_2 + O(\xi^3) \tag{17}$$

$$K_S = K_0. \tag{18}$$

These series will be valid as long as the conditions of (14)–(16) are satisfied. Substituting these series into the integral equation (10) results in the perturbation form of the integral equation (19)

$$\Phi(\chi) + 2\int_{-t}^{\infty} K_0(\chi,\chi') f(\chi')\, d\chi' + \xi \int_{-t}^{\infty} K_1(\chi,\chi') f(\chi')\, d\chi' + O(\xi^2) = 0. \tag{19}$$

A mode-matching technique is used to solve the integral equation. Thus, the Green's functions are written in terms of eigenfunctions so that the orthogonality relationships and completeness of the eigenfunctions can be used.

K_C is written in terms of the eigenfunctions $\Psi_{Cn}(\chi)$ and $\Psi_C(\chi,\gamma_b)$

$$K_C(\chi,\chi') = \sum_n A_n^2 \Psi_{Cn}(\chi)\Psi_{Cn}(\chi') + \int_0^\infty A_c^2(\gamma_b)\Psi_C(\chi,\gamma_b)\Psi_C(\chi',\gamma_b)\,d\gamma_b \quad (20)$$

where $\Psi_{Cn}(\chi)$ satisfies the cylindrical wave equation for discrete eigenvalues, $\lambda_n = k_{a,b}^2 - \nu_n^2$, and $\Psi_C(\chi,\gamma_b)$ satisfies the equation for the continuous spectrum of eigenvalues $\lambda_c = k_{a,b}^2 - \nu^2$ [12]. $\Psi_{Cn}(\chi)$ represents the discrete modes and $\Psi_C(\chi,\gamma_b)$ represents the continuous modes.

A_n^2 is an unknown constant and $A_c^2(\gamma_b)$ is an unknown function. These unknowns must be determined so that the Green's function will satisfy the source conditions (21) and (22) at $\chi = \chi'$ [6]

$$G_C(\rho,\rho')|_{\rho=\rho'+\Delta} = G_C(\rho,\rho')|_{\rho=\rho'-\Delta}, \quad \Delta \to 0 \quad (21)$$

$$\left.\frac{\partial G_C(\rho,\rho')}{\partial\rho}\right|_{\rho=\rho'+\Delta} - \left.\frac{\partial G_C(\rho,\rho')}{\partial\rho}\right|_{\rho=\rho'-\Delta} = \frac{-1}{\rho'}, \quad \Delta \to 0. \quad (22)$$

To derive the perturbation form of the eigenfunctions, the eigenfunctions and the discrete values ν_n are expanded in a perturbation series. The perturbation forms of the eigenfunctions can then be found by applying the perturbed coordinate system to the cylindrical wave equation, taking the Fourier transform of the wave equation with respect to s and then substituting the perturbation series expansions of the eigenfunctions and discrete eigenvalues into the equation. This results in a set of recursive equations for the discrete eigenfunctions and another set of recursive equations for the continuous eigenfunctions. These equations with the use of the boundary conditions can be solved successively for higher order terms of the perturbation expansion of the eigenfunctions.

After solving these equations, A_c and A_n are still unknown. Furthermore, each higher order discrete and continuous mode will add one further unknown. Thus, the zero order continuous and discrete mode each has one unknown, the first-order modes each have two unknowns and so on. In order to determine these unknowns, the source conditions on the Green's functions (21) and (22) must be applied.

The perturbation forms of the Green's functions expressed in terms of the perturbation form of the eigenfunctions are shown in (23) and (24). The eigenfunctions are presented in [9]

$$K_0(\chi,\chi') = \sum_n A_n^2 \Psi_{n0}(\chi)\Psi_{n0}(\chi') + \int_0^\infty A_c^2(\gamma_b)\Psi_0(\chi,\gamma_b)\Psi_0(\chi',\gamma_b)\,d\gamma_b \quad (23)$$

$$K_1(\chi,\chi') = \sum_n A_n^2[\Psi_{n0}(\chi)\Psi_{n1}(\chi') + \Psi_{n1}(\chi)\Psi_{n0}(\chi')] + \int_0^\infty A_c^2(\gamma_b)[\Psi_0(\chi,\gamma_b)\Psi_1(\chi',\gamma_b) + \Psi_1(\chi,\gamma_b)\Psi_0(\chi',\gamma_b)]\,d\gamma_b. \quad (24)$$

The following mode orthogonality relationships are used in the solution of the integral equation:

$$C_{n0,m0} = \int_{-t}^\infty R(\chi)\Psi_{n0}(\chi)\Psi_{m0}(\chi)\,d\chi = \frac{1}{2j\nu_{0n}A_n^2}\delta_{nm} \quad (25)$$

$$C_{n0,0} = \int_{-t}^\infty R(\chi)\Psi_{n0}(\chi)\Psi_0(\chi)\,d\chi = 0 \quad (26)$$

$$C_{0,0} = \int_{-t}^\infty R(\chi)\Psi_0(\gamma_b,\chi)\Psi_0(\tilde{\gamma}_b,\chi)\,d\chi = \frac{2\pi}{\varepsilon_b}\Gamma_D\Gamma_N\delta(\gamma_b - \tilde{\gamma}_b) \quad (27)$$

where

$$R(\chi) = \begin{cases} \frac{1}{\varepsilon_a} & -t < \chi < 0 \\ \frac{1}{\varepsilon_b} & \chi > 0. \end{cases}$$

The following integrals incorporating the zero- and first-order modes are also used:

$$C_{n0,1} = \int_{-t}^\infty R(\chi)\Psi_{n0}(\chi)\Psi_1(\nu,\chi)\,d\chi \neq 0 \quad (28)$$

$$C_{n1,0} = \int_{-t}^\infty R(\chi)\Psi_{n1}(\chi)\Psi_0(\nu,\chi)\,d\chi \neq 0 \quad (29)$$

$$C_{n0,m1} = \int_{-t}^\infty R(\chi)\Psi_{n0}(\chi)\Psi_{m1}(\chi)\,d\chi \neq 0. \quad (30)$$

These integrals are not equal to zero because the zero- and first-order modes are not orthogonal.

Finally, the incident field H_{zS}^{inc} can be written in terms of the mode functions

$$H_{zS}^{\text{inc}}(x,y) = \sum_n I_n^{\text{inc}} e^{-j\nu_{0n}y}\Psi_{n0}(x). \quad (31)$$

C. Integral Equation Solution

The modes for the straight surface—the zero-order modes—form a complete set [12]. Therefore, the the unknown [$f(x)$ in the integral equation (10)] can be expressed as a summation of these modes

$$f(\chi) = \sum_n \beta_n \Psi_{n0}^{(a,b)}(\chi) + \int_0^\infty \beta(\gamma_b)\Psi_0^{(a,b)}(\gamma_b,\chi)\,d\gamma_b. \quad (32)$$

As was done before, the unknowns β_n and $\beta(\gamma_b)$ are expanded in a perturbation series

$$\beta_n = \beta_{n0} + \xi\beta_{n1} + O(\xi^2) \quad (33)$$

$$\beta(\gamma_b) = \beta_0(\gamma_b) + \xi\beta_1(\gamma_b) + O(\xi^2). \quad (34)$$

The above equations are substituted into the integral equation and the orthogonality relationships are used to find the

unknowns β_{n0}, β_{n1}, $\beta_0(\gamma_b)$, and $\beta_1(\gamma_b)$

$$\beta_{n0} = -j\nu_{0n} I_n^{\text{inc}} \tag{35}$$

$$\beta_{n1} = -\nu_{0n} \sum_m I_m^{\text{inc}} A_n A_m \times [\nu_{0m} C_{m0,n1} + \nu_{0n} C_{n0,m1}] \tag{36}$$

$$\beta_0(\gamma_b) = 0 \tag{37}$$

$$\beta_1(\gamma_b) = \sum_n \nu_{0n} I_n^{\text{inc}} A_c^2(\gamma_b) \times [\nu C_{n1,0}(\gamma_b) + \nu_{0n} C_{n0,1}(\gamma_b)]. \tag{38}$$

The zero-order solution corresponds to the radius of curvature R approaching infinity. In other words, the geometry becomes an infinite plane with no discontinuity in curvature. In this case, the incident field will propagate across the aperture without any disruptions. Thus, as expected, $\beta_0(\gamma_b)$ is zero.

D. Fields

The field $H_z(x)$ is calculated using (7) and (8). This results in the following equations which are valid for $y \le 0$ and $s \ge 0$, respectively.

$y \le 0$

$$H_z^{(a,b)}(x,y) = \sum_n \left\{ I_n^{\text{inc}} e^{-j\nu_{0n} y} \Psi_{n0}^{(a,b)} + \xi j \sum_m I_m^{\text{inc}} A_n A_m \times [\nu_{0m} C_{m0,n1} + \nu_{0n} C_{n0,m1}] e^{-j\nu_{0n} y} \Psi_{n0}^{(a,b)} + \xi j I_n^{\text{inc}} \int_0^\infty A_c^2(\gamma_b) [\nu C_{n1,0}(\gamma_b) + \nu_{0n} C_{n0,1}(\gamma_b)] \Psi_0(\gamma_b, x) e^{j\nu y} \, d\gamma_b \right\} + O(\xi^2) \tag{39}$$

$s \ge 0$

$$H_z^{(a,b)}(\chi,s) = \sum_n \left\{ I_n^{\text{inc}} \Psi_{n0}^{(a,b)} e^{-j\nu_{0n} s} + \xi \left(j \sum_m I_m^{\text{inc}} A_n A_m \times [\nu_{0m} C_{m0,n1} - \nu_{0n} C_{n0,m1}] \Psi_{n0}^{(a,b)} e^{-j\nu_{0n} s} + I_n^{\text{inc}} \Psi_{n1}(\chi) e^{-j\nu_{0n} s} \right) + \xi j I_n^{\text{inc}} \int_0^\infty A_c^2(\gamma_b) \times [-\nu C_{n1,0}(\gamma_b) + \nu_{0n} C_{n0,1}(\gamma_b)] \times \Psi_0(\gamma_b, x) e^{j\nu s} \, d\gamma_b \right\} + O(\xi^2). \tag{40}$$

As expected, the zero-order term is an expression for an infinite straight surface.

The far-field pattern can be calculated by using saddle-point integration [6]. This results in (41). It should be noted that the radiation field is a first-order quantity in the perturbation variable $\xi = \frac{1}{R}$

$$H_z(r,\theta) \sim \xi j \sqrt{\frac{2\pi}{k_b r}} \sum_n I_n^{\text{inc}} \{ B_{<>} [\gamma_b \varepsilon_a \cos(\gamma_a t) - j\gamma_a \varepsilon_b \sin(\gamma_a t)] \} \nu e^{-jk_b r + j\frac{\pi}{4}} \Big|_{\substack{\gamma_{b<>} \\ \nu_{<>}}} \tag{41}$$

where $y < 0$

$$B_< = A_c^2(\gamma_b)(\nu C_{n1,0} + \nu_{0n} C_{n0,1})$$
$$\gamma_{b_<} = k_b \sin(\theta)$$
$$\nu_< = -k_b \cos(\theta)$$

$y > 0$

$$B_> = A_c^2(\gamma_b)(-\nu C_{n1,0} + \nu_{0n} C_{n0,1})$$
$$\gamma_{b_>} = k_b \sin(\theta)$$
$$\nu_> = k_b \cos(\theta).$$

IV. Results

Fig. 3 is a polar plot of the radiation pattern $|\hat{H}_z(\theta)|$ due to an incident zero-order mode on the curvature discontinuity for three different frequencies. $\hat{H}_z(\theta)$ is $H_z(r,\theta)$ multiplied by the radius of curvature of the curved section $R = \frac{1}{\xi}$ as defined in (42).

$$\hat{H}_z(\theta) = \frac{1}{\xi} \sqrt{\frac{k_b r}{2\pi}} e^{jk_b r} H_z(r,\theta). \tag{42}$$

The parameters for the plot are $\varepsilon_{ra} = 4$, $\mu_{ra} = 1$, $\varepsilon_{rb} = 1$, $\mu_{rb} = 1$, and $t = 1$ cm. Results for three different values of $\hat{\omega}$ are plotted where $\hat{\omega}$ is the frequency normalized by the cutoff frequency of the first mode as defined in (43)

$$\hat{\omega} = \frac{\omega t \sqrt{k_a^2 - k_b^2}}{\pi}. \tag{43}$$

For $\hat{\omega} = 0.25$, $I_0^{\text{inc}} = 2.85$; for $\hat{\omega} = 0.35$, $I_0^{\text{inc}} = 17.4$; and for $\hat{\omega} = 0.45$, $I_0^{\text{inc}} = 45$. Thus, as $\hat{\omega}$ increases, the magnitude of the incident field must also increase so that all three of the examples can appear on the same plot.

For the examples shown in Fig. 3, the frequency is less than half the first-mode cutoff frequency. For these cases, the maximum magnitude of the radiated field decreases as the frequency increases. This is because the incident field becomes more tightly bound to the surface at higher frequencies so that when the discontinuity is encountered less energy is radiated. It is also clear from Fig. 3 that as the frequency increases the angle of the the main lobe maximum direction increases. The reason for this can be understood in the following way. The fields on the aperture $y = 0$, $x > -t$ radiate into the region $y > 0$. At low frequencies, the field is loosely bound and spread out over the aperture. The radiation pattern for such a field is narrow and near the y axis. For higher frequencies, the mode is more tightly bound, confined to the region near the conductor and, therefore, the radiated energy is more spread out. As the frequency approaches a higher mode cutoff the above noted trends in direction and magnitude become more complicated as will be shown below.

Before proceeding to what occurs near higher mode cutoffs, the coated surface results are compared to published results for the similar problem of curvature changes in an impedance surface. Shevchenko [1] and Kuester and Chang [5] have solved this problem. It can be analytically shown that when the coated surface approximates an impedance surface, the solution for the coated surface reduces to their solution for an

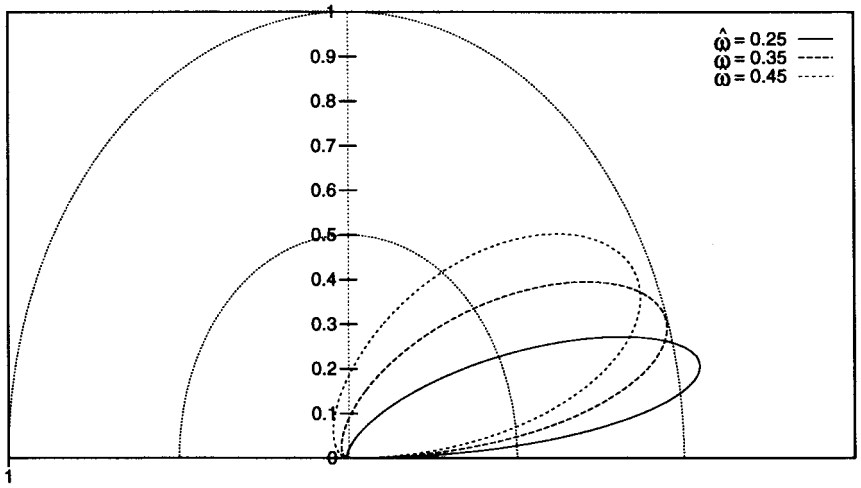

Fig. 3. A polar plot of $\hat{H}_z(\theta)$ for the coated surface solution. The parameters for the example plotted are: $\varepsilon_{ra} = 4$; $\mu_{ra} = 1$; $\varepsilon_{rb} = 1$; and $\mu_{rb} = 1$. Three scaling factors are used. For $\hat{\omega} = 0.25$, $I_0^{\rm inc} = 2.85$; for $\hat{\omega} = 0.35$, $I_0^{\rm inc} = 17.4$; and for $\hat{\omega} = 0.45$, $I_0^{\rm inc} = 45$.

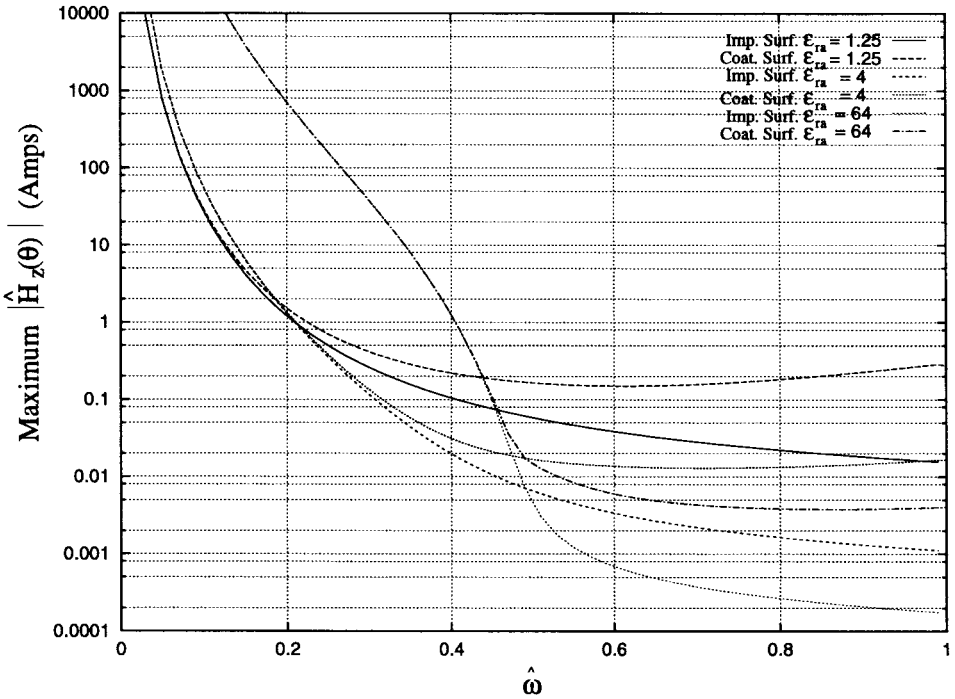

Fig. 4. The maximum magnitude of the main lobe of $\hat{H}_z(\theta)$ for the coated surface solution and the impedance surface solution as a function of $\hat{\omega}$. The parameters for the example plotted are $\mu_{ra} = 1$, $\varepsilon_{rb} = 1$, $\mu_{rb} = 1$, and $I_0^{\rm inc} = 1$.

impedance surface [9]. The conditions needed for the coated surface to approximate an impedance surface are that the thickness of the coating be small $\frac{t}{\lambda} \to 0$, where λ is the wavelength in the dielectric and that the dielectric constant of the coating ε_a be large. When these conditions are met, the surface impedance γ_0 is given by [14, eq. (44)]

$$\gamma_0 = -j\frac{\varepsilon_b \gamma_{a0}}{\varepsilon_a} \tan(\gamma_{a0} t). \tag{44}$$

Fig. 4 is a comparison of the maximum magnitude of the main lobe of the radiated field $\hat{H}_z(\theta)$ (42) as calculated using the impedance surface solution and the coated surface solution. These quantities are plotted as a function of the normalized frequency $\hat{\omega}$. Fig. 5 shows the angle (in radians) where this main lobe maximum occurs as a function of the normalized frequency. The parameters for the plot are $\mu_{ra} = 1$, $\varepsilon_{rb} = 1$, $\mu_{rb} = 1$, and $t = 1$ cm. The calculations are done for ε_{ra}, 1.25, 4, and 64.

For $\hat{\omega}$, less than about 0.5, the greatest difference between the impedance surface solution and the coated surface solution, is in the magnitude plot. The angle plots follow each other fairly closely until $\hat{\omega}$ is closer to 0.5 and then diverge dramatically.

It is known that as the thickness of the coating increases the impedance surface approximation becomes less accurate [14]. Because of this the two solutions diverge for larger values

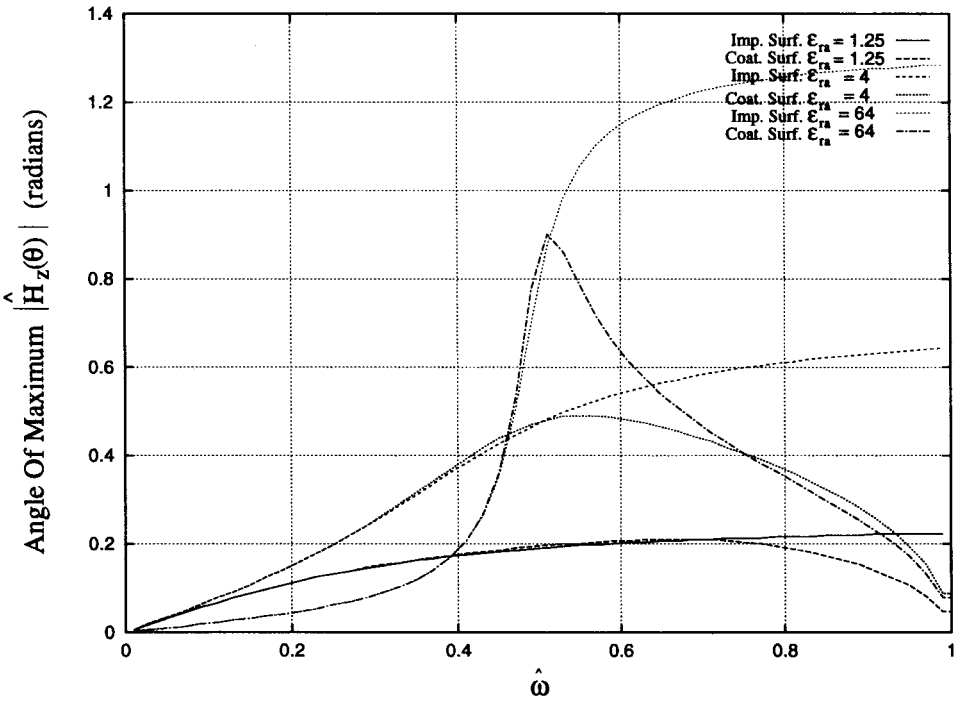

Fig. 5. The direction of the maximum magnitude of $\hat{H}_z(\theta)$ for the coated surface solution and the impedance surface solution in radians as a function of $\hat{\omega}$. The parameters for the example plotted are $\mu_{ra} = 1$, $\varepsilon_{rb} = 1$, $\mu_{rb} = 1$, and $I_0^{\rm inc} = 1$.

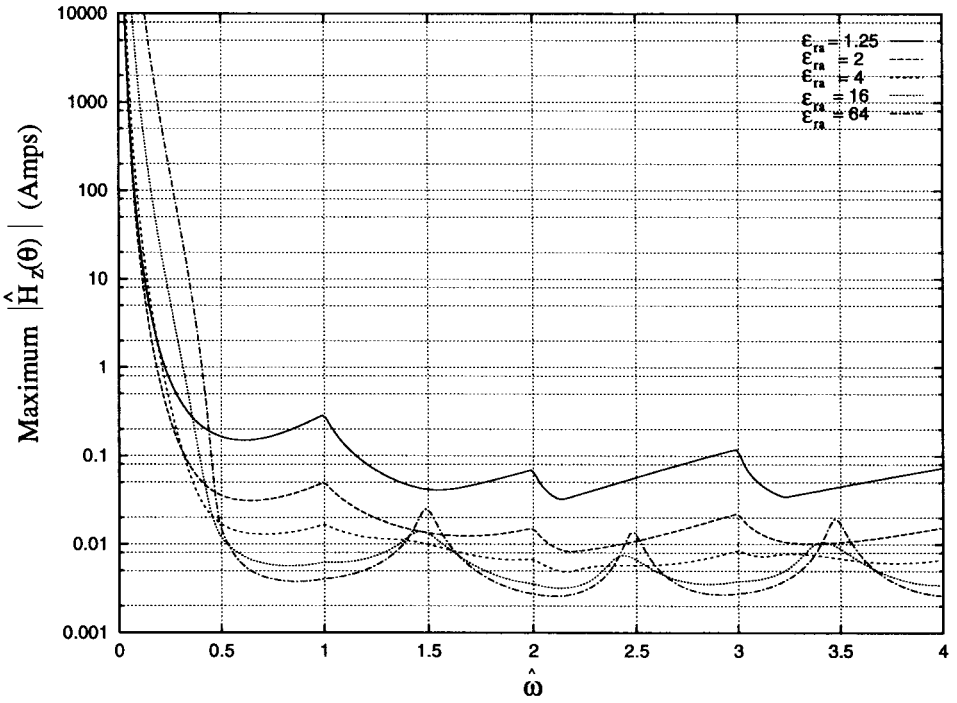

Fig. 6. The maximum magnitude of the main lobe of $\hat{H}_z(\theta)$ for the coated surface as a function of $\hat{\omega}$. The parameters for the example plotted in these figures are $\mu_{ra} = 1$, $\varepsilon_{rb} = 1$, $\mu_{rb} = 1$, $t = 1$ cm, $I_0^{\rm inc} = 1$, $I_1^{\rm inc} = 0$, $I_2^{\rm inc} = 0$, $I_3^{\rm inc} = 0$.

of $\hat{\omega}$. It is also known that as the dielectric constant of the coating becomes larger the impedance surface approximation becomes more accurate. Thus, for $\varepsilon_{ra} = 1.25$ the impedance surface and coated surface results diverge at about $\hat{\omega} = 0.1$, for $\varepsilon_{ra} = 4$ they diverge at about $\hat{\omega} = 0.3$, and for $\varepsilon_{ra} = 64$ they diverge at about $\hat{\omega} = 0.5$. It is important to note, though, that the coated surface results and impedance surface results match when the impedance surface approximation is valid.

Figs. 6 and 7 are plots, with respect to $\hat{\omega}$ of the maximum value of the radiated field $\hat{H}_z(\theta)$ and the direction of the maximum lobe of the radiated field, respectively. The incident field only consists of the $\rm TM_0$ surface wave $I_0^{\rm inc} = 1$. The

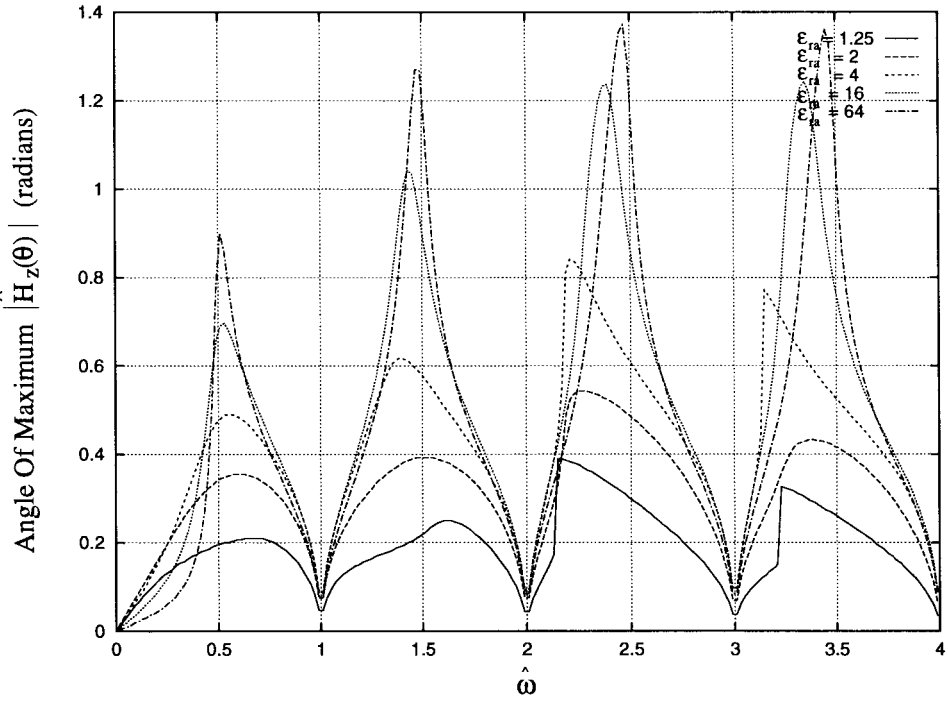

Fig. 7. The direction of the main-lobe maximum of $\hat{H}_z(\theta)$ for the coated surface as a function of $\hat{\omega}$. The parameters for the example plotted in these figures are $\mu_{ra} = 1$, $\varepsilon_{rb} = 1$, $\mu_{rb} = 1$, $t = 1$ cm, $I_0^{\rm inc} = 1$, $I_1^{\rm inc} = 0$, $I_2^{\rm inc} = 0$, $I_3^{\rm inc} = 0$.

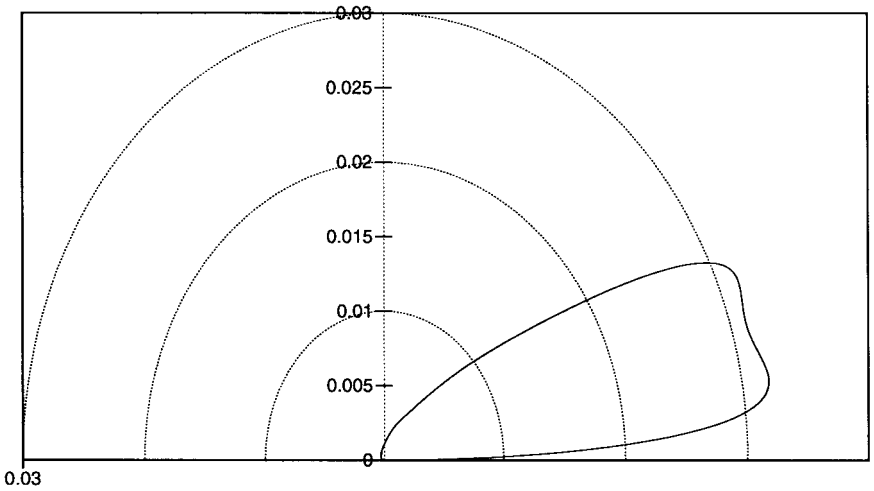

Fig. 8. A polar plot of the radiation pattern. The parameters for the example plotted in these figures are $\hat{\omega} = 2.13$, $\varepsilon_{ra} = 1.25$, $\mu_{ra} = 1$, $\varepsilon_{rb} = 1$, $\mu_{rb} = 1$, $t = 1$ cm, $I_0^{\rm inc} = 1$, $I_1^{\rm inc} = 0$, $I_2^{\rm inc} = 0$, $I_3^{\rm inc} = 0$.

other parameters for the plot are $\mu_{ra} = 1$, $\varepsilon_{rb} = 1$, $\mu_{rb} = 1$, and $t = 1$ cm. Curves for five different values of ε_{ra}, 1.25, 2, 4, 16, and 64, are shown.

As in Fig. 3 for $\hat{\omega} < 0.5$, the main-lobe maximum tends to become smaller and the angle of the maximum radiation becomes larger as the frequency becomes higher. For $\hat{\omega} > 1.0$, however, higher order bound modes are excited by the discontinuity. For instance, the discontinuity causes cross coupling of energy between the TM_0 incident field and the TM_1 field. This cross coupling is mathematically expressed in (36). Since both the TM_0 and TM_1 fields exist in the aperture, they both radiate into the region $y > 0$. Because the TM_1 field is less tightly bound near its cutoff, it radiates a narrow pattern primarily at small angles and dominates the radiation pattern. This small angle of radiation explains why the direction of the maximum angle of radiation is small near cutoff, as shown in Fig. 7. Between $\hat{\omega} = 0.5$ and $\hat{\omega} = 1.0$ the behavior is a continuous transition between single mode behavior and the behavior just above cutoff. This could probably be explained with a leaky wave model. Note further that this behavior repeats itself as $\hat{\omega}$ passes through higher order cutoff frequencies.

The magnitude plot (Fig. 6) shows another interesting characteristic. For small values of ε_{ra} (approximately $\varepsilon_{ra} < 2$) the magnitude increases near higher mode cutoffs, $\hat{\omega} = 1, 2, 3, \cdots$, and for larger values of ε_{ra} it increases midway

between higher mode cutoffs. At intermediate values of ε_{ra} (approximately $\varepsilon_{ra} = 4$) the magnitude increases both at the mode cutoffs and midway between mode cutoffs. These magnitude patterns are due to the phase relationships of the fields at the aperture of the curvature discontinuity.

Fig. 8 is a polar plot of the magnitude of $\hat{H}_z(\theta)$. The parameters for the plot are $\varepsilon_{ra} = 1.25$, $\mu_{ra} = 1$, $\varepsilon_{rb} = 1$, $\mu_{rb} = 1$, $t = 1$ cm, and $\hat{\omega} = 2.13$. The incident field only consists of the TM_0 surface wave but $\hat{\omega}$ was chosen so that the TM_0, TM_1, and TM_2 modes could be supported by the surface. Because the surface supports higher order modes and there is cross coupling of energy into these modes at the discontinuity, these higher order modes will contribute to the radiation pattern. Therefore, the radiation pattern is more complicated in this case than it was in the the single-mode case in Fig. 3.

V. Conclusion

The radiated field caused by a surface wave incident upon an abrupt but modest change in curvature of a dielectric-coated perfect conductor was found by formulating the problem as an integral equation. The integral equation was solved recursively through the use of regular perturbation theory. For thin coatings, this solution agreed with Shevchenko and Kuester and Chang's solution for an impedance surface. As expected, as the thickness of the surface increased the coated surface solution diverged from the impedance surface solution. For the example above, this divergence became large for frequencies above half the cutoff frequency of the first mode. It may be possible to improve the impedance surface solution through the use of higher order impedance boundary conditions [14]–[16], but these are still limited to a relatively thin coating. In order to examine what occurs as the cutoff of the higher order modes is approached and surpassed, the coated surface must be examined.

Modes tightly bound to the surface produce a wide radiation pattern. Modes loosely bound to the surface produce a narrow endfire radiation pattern. As the cutoff of the higher order modes is approached, energy is cross coupled into the higher order mode. Near cutoff, the higher order mode is loosely bound to the surface and, therefore, has a narrow endfire radiation pattern. This narrow pattern dominates the overall radiation pattern.

When ε_{ra} is small the magnitude near cutoff is large enough that the above mentioned trends should be measurable.

References

[1] V. V. Shevchenko, *Continuous Transitions in Open Waveguides*. Boulder, CO: Golem, 1971.

[2] V. H. Weston, "The effect of a discontinuity in curvature in high-frequency scattering," *IRE Trans. Antennas Propagat.*, vol. 10, pp. 775–780, 1962.

[3] ———, "The effect of a discontinuity in curvature in high-frequency scattering—Part II," *IEEE Trans. Antennas Propagat.*, vol. AP-13, pp. 611–613, July 1965.

[4] T. B. A Senior, "The diffraction matrix for a discontinuity in curvature," *IEEE Trans. Antennas Propagat.*, vol. AP-20, pp. 326–333, Mar. 1972.

[5] E. F. Kuester and D. C. Chang, "Scattering of a surface-wave from a curvature discontinuity on a convex impedance surface," *IEEE Trans. Antennas Propagat.*, vol. AP-25, pp. 796–810, June 1977.

[6] L. B. Felsen and N. Marcuvitz, *Radiation and Scattering of Waves*. New York: IEEE Press, 1994.

[7] J. W. Goodman, *Introduction To Fourier Optics*. New York: McGraw-Hill, 1968.

[8] R. F. Harrington, *Time-Harmonic Electromagnetic Fields*. New York: McGraw-Hill, 1961.

[9] D. H. Monteith, "Radiation due to a convex curvature discontinuity of a dielectric-coated perfect conductor," Ph.D. dissertation, School of Elect. Eng. Comput. Sci., Washington State Univ., Pullman, WA, Dec. 1996.

[10] E. F. Kuester and D. C. Chang, "Radiation of a surface wave from a curvature discontinuity in an impedance surface—Part I: Convex bend," Sci. Rep. no. 16, Electromagn. Lab. Dept. Elect. Eng., Univ. Colorado, Boulder, 1976.

[11] J. R. Wait, "Electromagnetic surface waves," in *Advances in Radio Research*. New York: Academic, 1964, vol. 1, pp. 157–217.

[12] G. Tyras, *Radiation and Propagation of Electromagnetic Waves*. New York: Academic, New York, 1969.

[13] L. A. Segal and C. C. Lin, *Mathematics Applied To Deterministic Problems In The Natural Sciences*. New York: Macmillan, 1974.

[14] T. B. A. Senior, "Approximate boundary conditions," *IEEE Trans. Antennas Propagat.*, vol. AP-29, pp. 826–829, May 1981.

[15] D. J. Hoppe and Y. Rahmat-Samii, "Higher order impedance boundary conditions applied to scattering by coated bodies of revolution," *IEEE Trans. Antennas Propagat.*, vol. 42, pp. 1600–1611, Dec. 1994.

[16] T. B. A. Senior and J. L. Volakis, "Derivation and application of a class of generalized boundary conditions," *IEEE Trans. Antennas Propagat.*, vol. 37, pp. 1566–1572, Dec. 1989.

David H. Monteith received the B.S. and M.S. degrees in electrical engineering from the University of Idaho, Moscow, ID, in 1986 and 1989, respectively, and the Ph.D. degree in electrical engineering from Washington State University, Pullman, in 1996.

He has worked in the areas of electromagnetic scattering, computational electromagnetics, antenna design, electromagnetic coupling, and system modeling.

Robert G. Olsen received the B.S. degree in electrical engineering from Rutgers University, New Brunswick, NJ, in 1968, and the M.S. and Ph.D. degrees in electrical engineering from the University of Colorado, Boulder, in 1970 and 1974, respectively.

He has been a Faculty Member of the Electrical Engineering Department, Washington State University, Pullman, since 1973. He was a Visiting Scientist at GTE Laboratories, Waltham, MA, in 1980 and ABB Corporate Research, Västerås, Sweden, from 1984 to 1985. He was also a Visiting Professor at the Technical University of Denmark, Lyngby, in 1990. His research interests include electromagnetic interference from power lines, the electromagnetic environment of power lines, electromagnetic compatibility, and electromagnetic scattering.

Dr. Olsen is an Associate Editor of the IEEE Transactions on Electromagnetic Compatibility.